Lowering the Exponential Wall: Accelerating High-Entropy Alloy Catalysts Screening using Local Surface Energy Descriptors from Neural Network Potentials

Tomoya Shiota,[1,2,*] Kenji Ishihara,[2,†] and Wataru Mizukami[1,2,‡]

[1] *Graduate School of Engineering Science, Osaka University, 1-3 Machikaneyama, Toyonaka, Osaka 560-8531, Japan*

[2] *Center for Quantum Information and Quantum Biology, Osaka University, 1-2 Machikaneyama, Toyonaka 560-8531, Japan*

(Dated: April 15, 2024)

Computational screening is indispensable for the efficient design of high-entropy alloys (HEAs), which hold great potential for catalytic applications. However, the chemical space of HEAs is exponentially vast with respect to the number of constituent elements, and even screening calculations using machine learning potentials can be enormously time-consuming. To address this challenge, we propose a method to rapidly construct models that predict the properties of HEAs from data on monometallic systems (or few-component alloys). The core of our approach is a newly-introduced descriptor called local surface energy (LSE), which reflects the local reactivity of solid surfaces at atomic resolution. We successfully created a model using linear regression to screen the adsorption energies of molecules on HEAs based on LSEs from monometallic systems. Furthermore, we made high-precision model development by employing both classical machine learning and quantum machine learning. Using our method, we were able to complete the adsorption energy calculations of CO molecules on 1000 patterns of quinary nanoparticles consisting of 201 atoms within a few hours. These calculations would have taken hundreds of years and hundreds of days using density functional theory and a neural network potential, respectively. Our approach allows accelerated exploration of the vast chemical space of HEAs facilitating the design of novel catalysts.

I. INTRODUCTION

High-entropy alloys (HEAs), composed of five or more elemental species in concentrations ranging from 5 to 35 at%, have emerged as versatile materials with promising applications in catalysis and functionality[1–4]. Their rich compositional diversity paves the way for the "cocktail effect", unveiling unexpected properties that often surpass traditional single-element systems[3, 5]. Recent advancements highlight their superior catalytic performance[6–9], but the vast array of potential element combinations poses a significant challenge for experimental exploration.

Addressing this complexity, researchers have turned to computational methods for efficient screening[9–12]. First-principles calculations, such as density function theory (DFT)[13–15], coupled cluster (CC) theory[16–18] and many-body perturbation theory (MBPT)[19, 20], describe chemical reactions on solid surfaces with high accuracy. Volcano plots, derived from first-principles calculations, illustrate the optimal adsorption energy range for catalytic activity, balancing between excessively strong and weak interactions [12, 21, 22]. However, the heterogeneous surfaces of HEAs complicate the application of these models due to the varied adsorption sites, rendering conventional approaches computationally intensive.

To circumvent these limitations, neural network potentials (NNPs), which are based on the Behler-Parrinello framework [23–27] and graph neural networks [28–31], offer a promising solution. The universal NNP, capable of encompassing extensive elemental diversity, achieves high computational efficiency while maintaining accuracy on par with density functional theory (DFT) [29, 30, 32–44]. Very recently, NNPs specialized for HEA have emerged that are lightweight with transition learning [45]. Thus, recent advancements in refining NNPs have expedited catalytic property predictions, yet the necessity of evaluating all potential adsorption sites remains a computational bottleneck.

In contrast, descriptor-based machine learning models offer scalability by predicting adsorption energies through generalized coordination numbers and d-band centers, bypassing direct energy assessments [46–50]. Along with the coordination number descriptor, a model is also proposed to predict the adsorption energies of the remaining candidates by regressing the adsorption energies actually obtained from several first-principles calculations [10]. Nonetheless, their applicability to HEAs is hampered by the complexities of alloy compositions and the dependency on extensive first-principles calculations.

To address these challenges, we propose a methodology for predicting molecular adsorption energies on HEAs without direct adsorption energy computations. Our approach centers on a new descriptor, the local surface energy (LSE), reflecting the local reactivity of solid surfaces with atomic resolution. The LSE can be efficiently calculated using atomic energies from NNPs, facilitating rapid and comprehensive evaluations of catalytic properties. We validate our method through DFT comparisons,

* These two authors contributed equally to this work. E-mail at: shiota.tomoya.ss@gmail.com

† These two authors contributed equally to this work. E-mail at: ishihara-ke@office.osaka-u.ac.jp

‡ E-mail at: mizukami.wataru.qiqb@osaka-u.ac.jp

predicting adsorption energies for CO on IrPdPtRhRu HEA nanoparticles (NPs). Furthermore, we present a correction technique for adsorption energy, employing both classical and quantum-classical hybrid algorithms, enhancing the precision of our predictions.

II. METHODS

A. Local Surface Energy

The LSE metric is defined as follows:

$$LSE \equiv E_{\mathrm{at}}^{\mathrm{surf}} - E_{\mathrm{at}}^{\mathrm{bulk}}, \tag{1}$$

where $E_{\mathrm{at}}^{\mathrm{surf}}$ and $E_{\mathrm{at}}^{\mathrm{bulk}}$ denote the atomic energies in the surface and bulk environments, respectively. The LSE quantifies the energy loss by a single atom in the bulk environment when exposed to a surface. This definition enables the determination of surface stability even for surfaces in complex environments and multicomponent systems. The atomic energies in Equation (1) can be evaluated using the energy density analysis (EDA) from first-principles calculations such as DFT[52–56]. EDA is accurate because it is based on first-principles calculations, but it is not suitable for exhaustive calculations such as those in this study because of its high computational cost. Therefore, in this study, all LSEs were evaluated using NNPs. In Behler-Parrinello type NNP frameworks, the total energy E_{tot} of a system consisting of N atoms is evaluated as a sum of the energies of each atom:

$$E_{\mathrm{tot}} = \sum_{i=1}^{N} E_{\mathrm{at}}^{i}. \tag{2}$$

Yoo et al. demonstrated the ability to map atomic energies obtained by NNPs onto NP and surface systems [57]. NNP allows for a very efficient evaluation of LSEs because the atomic energies of all adsorption sites in one system can be obtained in a single calculation.

B. CO Molecule Adsorption on NPs

To investigate the effectiveness of LSE values in predicting surface reactions, we targeted the on-top adsorption energies of a CO molecule on various monometallic NPs, as a precursor to developing predictive models for high entropy alloys (HEAs). The NPs were truncated octahedron type corresponding to M_n, n=38, 79, 116, 201. The elements were platinum-group metals (PGMs) $\mathrm{M} = \mathrm{Ir}, \mathrm{Pd}, \mathrm{Pt}, \mathrm{Rh}, \mathrm{Ru}$. For the on-top adsorption of CO molecule on M_{201}, only the irreducible adsorption sites were computed, represented by the black line in Figure 1(a).

The adsorption energy E_{ad} was evaluated as

$$E_{\mathrm{ad}} = E_{\mathrm{tot}}^{\mathrm{CO/M_n}} - E_{\mathrm{tot}}^{\mathrm{CO}} - E_{\mathrm{tot}}^{\mathrm{M_n}}, \tag{3}$$

where $E_{\mathrm{tot}}^{\mathrm{CO/M_n}}$, $E_{\mathrm{tot}}^{\mathrm{CO}}$, and $E_{\mathrm{tot}}^{\mathrm{M_n}}$ denote the total energies of $\mathrm{CO/M_n}$, CO, and $\mathrm{M_n}$, respectively, as shown in Figure 1(b).

C. Regression of Adsorption Energy

The LSEs were calculated from the atomic energies of the monometallic bulk and monometallic NP surfaces, as shown in (i) of Figure 1(c). Next, we plotted the adsorption energy E_{ad} as a function of LSE at each adsorption site of monometallic NPs. Then, the correlation between adsorption energy E_{ad} and LSE was examined through the least-squares linear regression for each type of elemental monometallic NP, illustrated in (ii) of Figure 1(c). These regressions $E_{\mathrm{ad}}^{\mathrm{M}}$(Predict.) were utilized as predictive models to predict the adsorption energy of CO on the IrPdPtRhRu HEA NPs, as

$$E_{\mathrm{ad}}^{\mathrm{M}}(\mathrm{Predict.}) = \alpha_{\mathrm{M}} \times LSE + \beta_{\mathrm{M}}. \tag{4}$$

Here, α_{M} and β_{M} denote the regression coefficient and constant for each element monometallic NP, respectively. α_{M} represents the magnitude of the adsorption energy response to a change in LSE. β_{M} represents the adsorption energy of CO molecules when LSE is 0, in other word, when the surface atom have the same energy as that in the bulk environment.

D. Prediction of Adsorption Energy on HEA NPs

We predicted the adsorption energy of CO on IrPdPtRhRu HEA NPs using regressions $E_{\mathrm{ad}}^{\mathrm{M}}$(Predict.). Specifically, we calculated the adsorption energy of the CO molecule using only the LSE values. In general, the LSE of an atom at the adsorption site may be stabilized or destabilized by the surrounding environment. Therefore, in the complex environment involving multiple systems and NPs, the adsorption energy has a value different from that of a monometallic system[10, 58, 59]. We modeled IrPdPtRhRu as a truncated octahedron $\mathrm{IrPdPtRhRu_{201}}$, similar to those in the unitary system. The number of atoms was set as 40 for the four elemental species and 41 for the remaining one, and the arrangement of the elements was random, resulting in 20 structures of PGM-HEA NPs. The adsorption site of the CO was on-top only, as in the unitary system. Figure 1(c) illustrates the on-top adsorption of CO onto a corner Ru atom as an example.

The LSE prediction for adsorption sites in unitary NPs and CO adsorption energy in unitary systems through linear regression assumes a similar relationship between atomic-level stability and adsorption energy at the surface of HEA NPs. However, in HEAs, unexpected nonlinear behavior may be observed. Therefore, we constructed a corrected machine learning model for the LSE-derived adsorption energy, which learns the nonlinear relationship between the adsorption energy directly

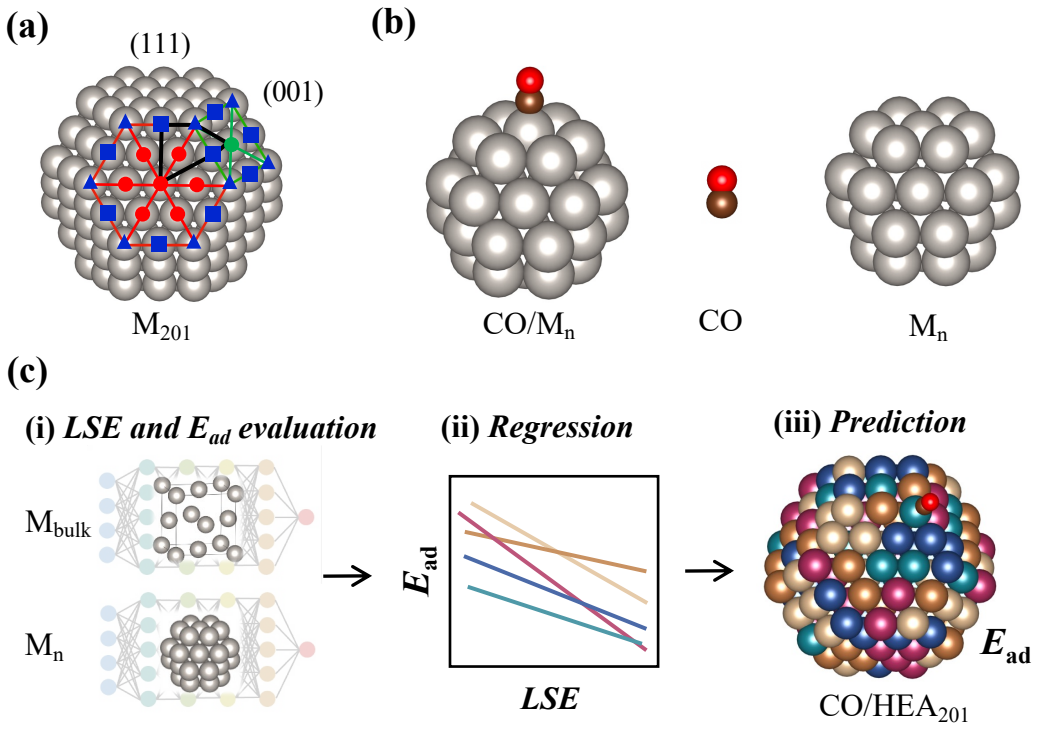

Figure 1. (a) 201 atom truncated octahedron NP and irreducible adsorption site of its surface atoms (black line). Circles, squares, and triangles indicate facet, edge, and corner sites on HEA_{201}, respectively. (b) On-top adsorption of CO molecules on NPs and the corresponding isolated systems. (c) Process flow of the proposed approach: (i) calculation of *LSE*s and adsorption energies, (ii) regression of adsorption energy for each atomic species on *LSE*, and (iii) prediction of adsorption energy using regressions. All geometries are visualized using VESTA3 [51], with a consistent color assignment for each atom.

obtained using the NNP for validation and the *LSE*-predicted adsorption energy obtained by the scheme in Figure 1. Kernel ridge regression (KRR) with a regularization function to suppress overfitting was employed as the nonlinear regression method. In addition, nonlinear regression using quantum machine learning, with high expressive power and a regularization function, was incorporated using a high-speed quantum simulator. For regression based on quantum machine learning, we introduced quantum circuit learning (QCL) proposed by Mitarai et al [60]. QCL is known to correspond to neural networks in conventional computers. In this study, we refer to this regression method as quantum neural network regression (QNNR). Details of KRR and QNNR are presented in the following text, and the degree of accuracy of adsorption energies by both models is discussed in Section III.

III. COMPUTATIONAL DETAILS

A. Modeling

We modeled CO adsorption on NPs, CO/M_n, using the Atomic Simulation Environment (ASE) [61, 62]. The initial lattice constants (LCs) for M_n were determined from bulk calculations. In the case of HEA_{201}, the largest LC in the bulk was used as the initial LC. A 15 Å vacuum region was inserted in all supercells to minimize cell-to-cell interactions. The initial structures of CO/M_n and CO/HEA_{201} were derived by placing CO on the on-top sites of the optimized structures of M_n and HEA_{201}, respectively, with the distance between the C atom and the adsorption site metal atom M set as 2 Å.

B. NNP Calculations

The NNP was M3GNet, a pre-trained model based on a graph neural network capable of computing periodic tables [34]. The crystal structures of the bulk $M = Ir, Pd, Pt, Rh, Ru$ were assumed to face-centered cubic (fcc). Although Ru exhibits the hcp form at room temperature, Ru with fcc structure can be created in NPs

Table I. Atomic energy and lattice constant of each bulk.

fcc bulk M	Ir	Pd	Pt	Rh	Ru
E_{at}^{bulk}(eV)	-8.941	-5.185	-6.069	-7.394	-9.305
LC (Å)	3.875	3.957	3.977	3.850	3.815

[63]. The atomic energy of bulk fcc metal M was determined using the energy corresponding to the minimum value obtained when varying the LC of the material in intervals of approximately 0.01 Å. The resulting atomic energy values and corresponding lattice constants are summarized in Table I. The Broyden–Fletcher–Goldfarb–Shanno (BFGS) algorithm was used for structural optimizations, with a max step of 0.005 Å. In the CO/M and CO/HEA structure optimization calculations, the M and HEA structures were fixed as stable structures of the isolated systems, respectively. Only the CO and adsorption site atom were relaxed with the constraint that the adsorbed molecules occupy the on-top site. Structural optimizations were performed until the force acting on each atom was 0.001 eV/Å.

C. DFT Calculations

DFT calculations were performed using the Vienna ab initio simulation package (VASP), version 5.4.4 [64–66]. We employed the Perdew–Burke–Ernzerhof generalized gradient approximation functional as the exchange-correlation functional[67]. Core electrons were treated using the projector augmented wave method [68, 69]. The electronic structures were optimized using the blocked Davidson iteration scheme within the spin-restricted approximation. The cutoff energy for plane wave functions was set as 400 eV. The ion geometries were optimized using the conjugate gradient algorithm with a convergence threshold of 0.01 eV/Å.

D. Nonlinear Regressions

KRRs were executed using scikit-learn version 1.2.2 [70]. The Gaussian kernel was chosen as the kernel function of the KRR. The hyperparameters for each model were optimized over 100 iterations of randomized search.

QNNRs were implemented using scikit-qulacs version 0.5.0[71]. Qulacs version 0.5.6 was used as the quantum circuit simulator[72]. The number of qubits in the QNNR model was 4. The number of iterations of the parameterized variational quantum circuit of the model corresponding to the weights of the neural network was 6. The time step for the time-evolution operator in parameterized variational quantum circuits was set as 0.5. The BFGS algorithm was used to update the parameters of the QNNR model.

IV. RESULTS

A. Correlation Between Adsorption Energy and LSE

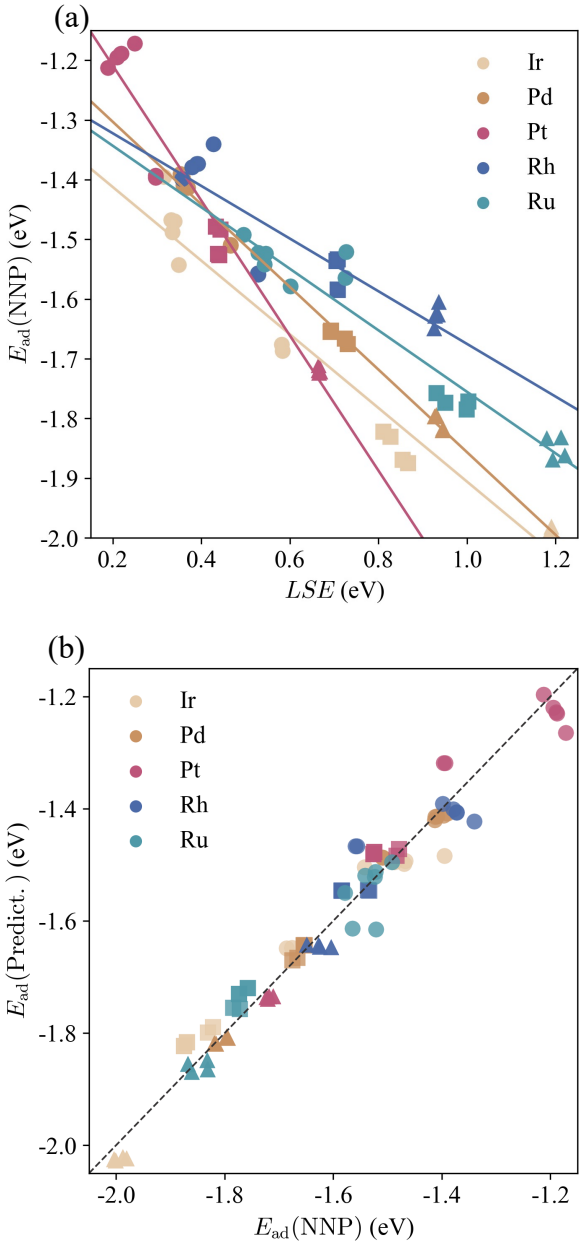

Figure 2. (a)Adsorption energies of CO calculated using the NNP for each adsorbed on-top site of M_n against the local surface energy (LSE). Solid lines represent the linear regressions of the adsorption energies of a CO molecule at the on-top sites in each element unitary system according to Equation (4). (b) Correlation between adsorption energies calculated directly by NNP and those predicted through regression. Circles, squares, and triangles at each datapoint represent the facet, edge, and corner CO adsorption sites, respectively.

The correlation between the LSE and CO adsorption energy E_{ad}(NNP) of the monometallic NPs obtained by the NNP is shown in Figure 2(a). Solid lines represent the linear regressions of the adsorption energies of a CO molecule at the on-top sites in each element unitary system, obtained using Equation (4). For all metal elements, the relationship between the adsorption energy E_{ad}(NNP) of CO molecule on-top site and LSE is linear. This outcome indicates that the adsorption energies of CO on a monometallic NP can be predicted if the LSE of each atom on the NP surface prior to molecular adsorption is known. The LSE of all adsorption sites for all elements ranges from approximately 0.2 to 1.2 eV. In other words, in all cases, the atomic energies are more unstable in the surface environment than in the bulk environment, which is reasonable given the lower coordination number in the surface environment. The adsorption energy E_{ad}(NNP) ranges from approximately -1.2 to -2.0 eV. Next, we focus on the adsorption sites of the NPs. For all elements, the adsorption energy exhibits the following decreasing order: facet, edge, and corner. Conversely, the LSE values increase in the order of facet, edge, and corner. The LSE values and adsorption energies are concentrated at the facet, edge, and corner, and an energy gap exists between each group of adsorption sites. The correlation between E_{ad}(NNP) and E_{ad}(Predict.) is shown in Figure 2.(b). The RMSE is 0.035 eV, revealing a strong correlation between LSE and adsorption energy. Verification of this adsorption energy via DFT calculations is described in Section III. C.

B. Prediction of the Adsorption Energy on HEA NPs

The LSE regressions based on Equation (4), as shown in Figure 1, are used to predict the adsorption energies of a CO molecule on the on-top sites of IrPdPtRhRu HEA NPs with truncated octahedral structures (HEA_{201}). To this end, 1000 patterns of HEA_{201} NPs are generated, and LSEs of the 122 atoms of the topmost surface layer present in each of them are evaluated. Figure 3(a) shows the 122,000 LSE values for each element and their total distribution. This distribution becomes smoother and converges as the number of NP patterns increases. The sum of all elements shown in gray in Figure 3(a) can be considered an indicator reflecting the reactivity of the entire HEA NP surface. In the monometallic system, the LSE ranges from approximately 0.2 to 1.2 eV. However, in the quintic HEA environment, these values undergo significant changes and span from approximately -0.1 to 2.4 eV. The distribution of each element exhibits two prominent peaks. For Pt and Pd, the LSE exhibits a major peak near 0 eV (or slightly lower energy), indicating greater stability compared with that in the monometallic environment. Notably, an LSE value of 0 corresponds to the energy of the bulk environment. The second, smaller peak remains nearly unchanged for Pd, whereas the LSE range expands by approximately 0.3 eV for Pt. In the case of Ir and Ru, the LSE value shifts toward higher energies compared with those in the monometallic systems. As for Rh, a slight increase in the LSE range is observed, lying between those for the stable Pt and Pd groups and less stable Ir and Ru groups.

Figure 3(b) illustrates the predicted adsorption energy of CO on all on-top sites of 1000 HEA_{201} NPs obtained using Equation (4) with LSE values. The range of on-top adsorption energy E_{ad} for CO on the monometallic system (Figure 2) expands by approximately 0.8 eV, from approximately -2.0 to -1.2 eV to -2.5 to -0.9 eV. This outcome serves as an example of how the adsorption characteristics diversify within a quintic HEA environment. The distribution of adsorption energies on each element also exhibits two prominent peaks. Next, we examine the differences among each elemental species. For Pd and Pt, the LSE values are very close, but the range of adsorption energies is broader on the high-energy side by 0.2 eV for Pt. A similar trend is observed for Ir and Ru on the low-energy side. In the case of Rh, a slight extension in the range of both high- and low-energy sides is observed, compared with that for the monometallic system. In particular, the adsorption energy is concentrated in three adsorption site groups (corner, edge, and facet) in the monometallic NP environment, but these groups take on more diverse values in the HEA NP environment. This representation as a distribution can help visualize the potential cocktail effect.

C. Verification of the LSE Predictions

The adsorption energy predicted using LSE is compared with the adsorption energies of CO on HEA_{201} directly calculated using the NNP and DFT. We limit the comparison to 2440 sites, encompassing all on-top sites across the 20 structures. In general, calculating the adsorption sites for all 1000 HEA_{201} configurations is a computationally intensive task, even with the assistance of NNP. The computation times using NNP and DFT are summarized in Table II. In the computing environment used in this study, the computation time per structural optimization step is approximately 1000 times less with NNP than that with DFT. However, the time required to perform direct structural optimization of the 122,000-site adsorption structure shown in the previous section with NNP would take 171 days, with DFT calculations expected to take 188 years. In contrast, the adsorption energy prediction using LSE takes only 1.4 days.

Figures 4(a) and (b) show the adsorption energies calculated directly by NNP and their predicted values. The RMSE is 0.150 eV, larger than that in the unitary system. However, a strong correlation can be observed between the LSE and adsorption energy in HEA, indicating that the adsorption energy in the multicomponent environment can be effectively predicted, as shown in Figure

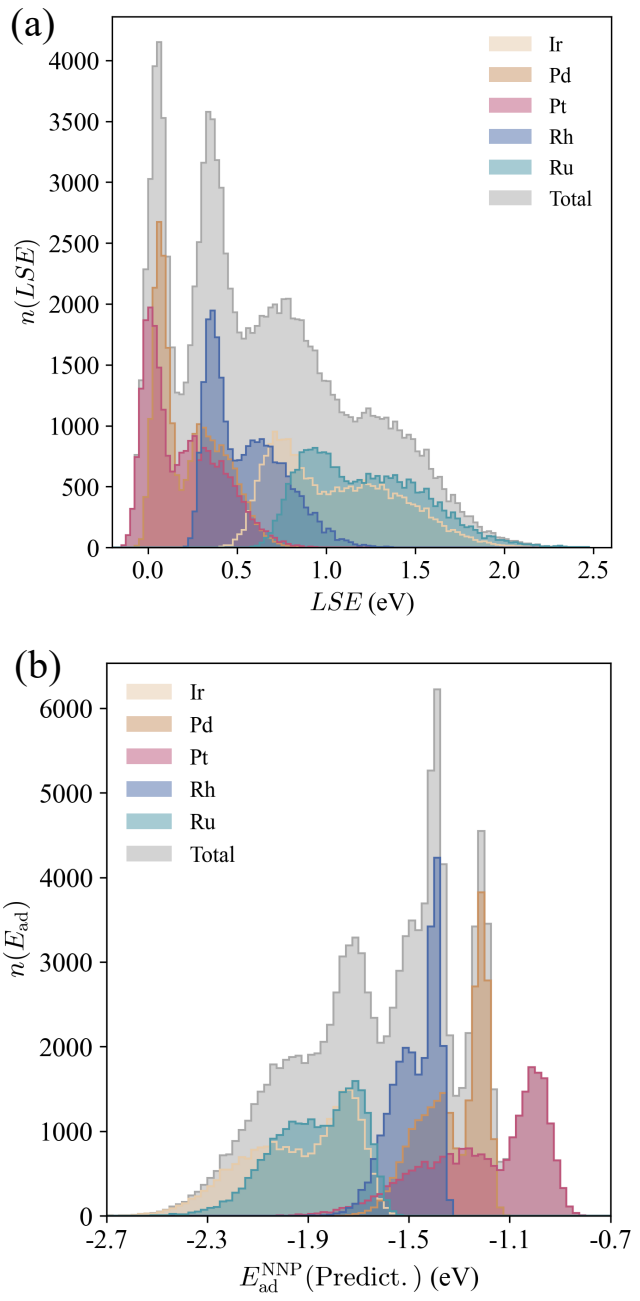

Figure 3. (a)Distributions of 122,000 *LSE* values of all topmost layer atoms of the 1000 structure-optimized HEA_{201} for each element and their sum, respectively. (b) Distributions of adsorption energies of CO for all on-top adsorption sites predicted using *LSE*s in (a) and Equation (4).

4(b). This finding suggests that the *LSE* can efficiently and accurately predict adsorption energies not only for unitary systems but also for complex multi-systems such as HEAs. Notably, when using the adsorption energy range of -2.0 to -1.2 eV in the unitary system as the interpolation region for E_{ad}(Predict.), the predictions are more reliable than those with other ranges. In the extrapolation region of E_{ad}(Predict.), the difference with E_{ad}(NNP) increase, and a maximum shift of approximately 0.5 eV can be observed.

Next, we explore the results for each elemental species. For all elemental species, the predicted adsorption energies become less accurate toward the low-energy side

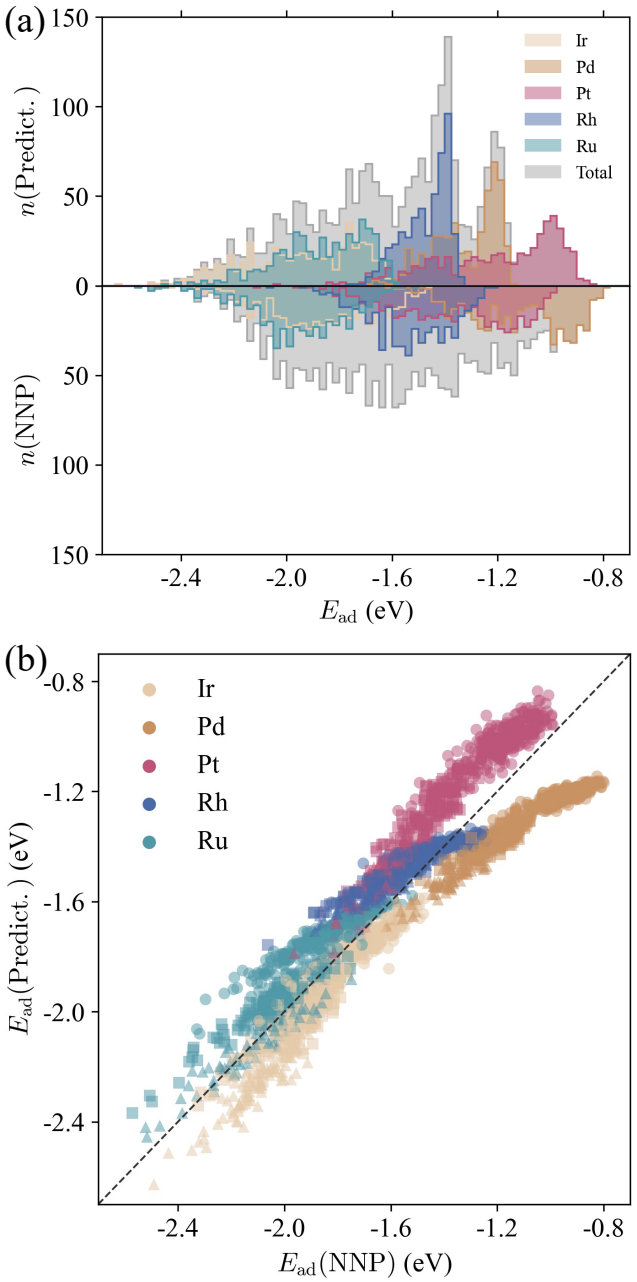

Figure 4. (a)Comparison and (b) correlation between the predicted adsorption energy via *LSE* and directly calculated adsorption energy of CO/HEA_{201} by the NNP. We limit the comparison to 2440 sites, encompassing all on-top sites across the 20 structures.

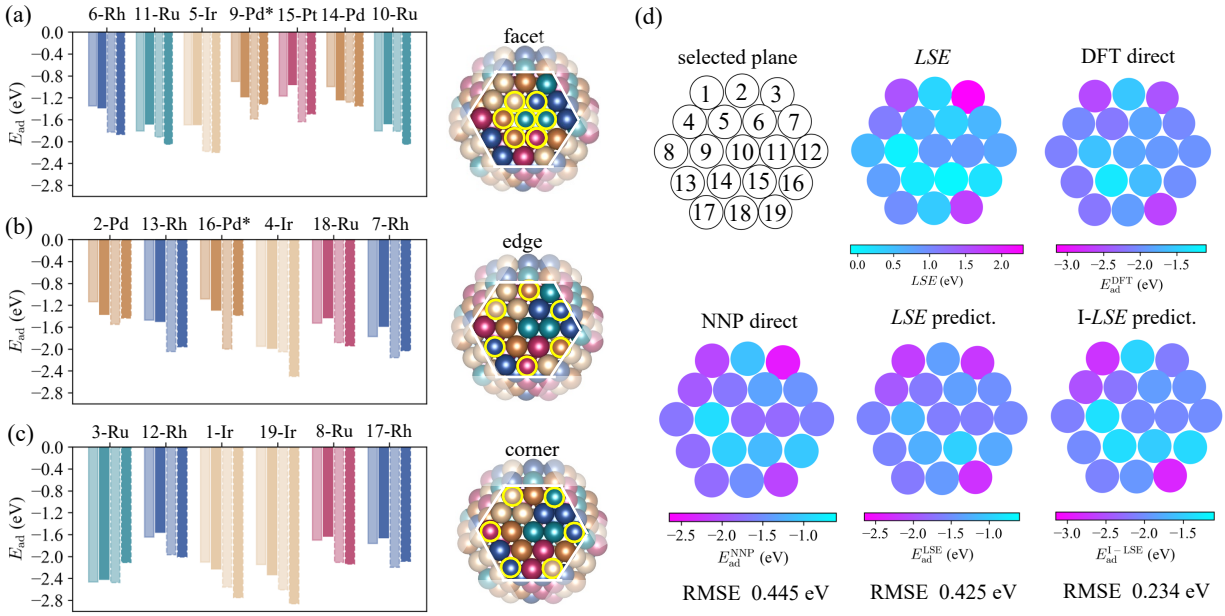

Figure 5. Bar graphs in (a), (b), and (c) show the evaluated adsorption energies of CO on the (111) plane of a randomly selected HEA_{201} at each on-top site of the facet, edge, and corner, respectively. The atoms of the selected plane are numbered as shown in (d). For each adsorption site, from left to right, the bar graph represents the adsorption energy obtained by direct evaluation using NNP (NNP direct), *LSE* prediction (*LSE* predict.), DFT, and *LSE* prediction parameterized by DFT data (I-*LSE* predict.). (d) illustrates the mapping of the *LSE* values of the atoms on the selected plane and corresponding adsorption energies shown in (a), along with the RMSE values relative to the DFT results. The asterisk indicates that the results of the structural optimization converge on the bridge site rather than the on-top site.

(Figure 4(a)). Figure 4(b) shows that for all elemental species, the adsorption energies are nonlinearly estimated toward the low-energy side. Additionally, the nonlinear region is dominated by the facet site adsorptions. Compared with sites with a low coordination number, such as corner and edge sites, the atoms on the facets are coordinated with eight or nine atoms. This increased coordination number renders them more sensitive to the surrounding environment compared to unitary systems. Consequently, the complex environment of HEA may introduce unexpected nonlinearity in the predictions. A potential solution to this problem is discussed in the subsequent section.

Finally, the accuracy of adsorption energy predictions is verified using NNP and *LSE* with DFT calculations, while seeking to enhance the prediction accuracy. In our computing environment, the computation cost of the adsorption energy evaluation by DFT is approximately 10^3 times that based on NNP, as indicated in Table II. Therefore, we randomly select one of the 20 structures of HEA_{201} discussed above and evaluate the adsorption energy for 19 sites on the (111) plane shown on the right side of Figure 5. The selected HEA_{201} is $Ir_{40}Pd_{40}Pt_{41}Rh_{40}Ru_{40}$. First, the inherent performance differences between NNP and DFT are compared based on direct NNP and DFT calculations without *LSE* predictions. The RMSE of adsorption energy for all sites obtained by NNP and DFT is 0.445 eV. The RMSE value of the *LSE* prediction based on DFT is 0.425 eV, corresponding to a slightly reduced accuracy (0.020 eV) compared with direct evaluation by NNP. However, the performance is comparable to the evaluation based on the NNP. Because this error is an order of magnitude larger than the chemical accuracy of 0.027 eV, methodologies and guidelines are needed to reduce the prediction error.

To address this accuracy problem, we determine the

Table II. Computational costs for 19 geometry optimizations of CO adsorption on the (111) plane on $Ir_{40}Pd_{40}Pt_{41}Rh_{40}Ru_{40}$ HEA NP by NNP and DFT.

	total time[s]	total step[step]	s/step
NNP[a]	2314	10480	0.22
DFT[b]	925518	5008	184.81
NNP/DFT[c]	3×10^{-3}	2	1×10^{-3}

[a] NNP calculations with M3GNET were performed using an AMD EPYC 7532 32-core Processor with 64 CPUs.
[b] DFT calculations with VASP were performed using 10 Intel(R) Xeon(R) Platinum 9242 CPUs with 96 CPUs in mpi parallel, resulting in 960 CPUs.
[c] NNP/DFT represents the ratio of values obtained using the NNP to that calculated using DFT.

Table III. Atomic energy and lattice constant of each bulk.

	Ir	Pd	Pt	Rh	Ru
α(DFT)	-0.639	-0.446	-1.073	-0.345	-0.041
α(NNP)	-0.617	-0.692	-1.131	-0.441	-0.515
β(DFT)	-1.782	-1.305	-1.521	-1.755	-2.012
β(NNP)	-1.289	-1.165	-0.983	-1.234	-1.240

linear regression parameters of Equation (4), as in the previous section, using the adsorption energy obtained from the DFT calculation. The determined regression parameters are shown in Table III. Comparing the adsorption energy values from the DFT-parametrized *LSE* (I-*LSE*) prediction with those from the direct DFT calculation reveals a significant improvement in prediction performance, with an RMSE of 0.234 eV, representing a reduction in energy error by half. This outcome demonstrates the potential of improving adsorption energy prediction performance with *LSE*. In the next section, we discuss methodologies and guidelines for enhancing the accuracy of forecasts using *LSE*. Figure 5 (d) shows a color map of the *LSE* value, adsorption energy computed from DFT, and adsorption energy predicted by each method. Although the RMSE values deviate significantly from DFT prediction, the qualitative energy relationship is accurately captured. This suggests that *LSE* prediction can also be used as an efficient modeling tool for accurate computations.

D. Solution to the nonlinearity problem

We introduce linear regression to predict the adsorption energy of the CO molecule on the on-top sites in the monometallic system as a function of the *LSE* index derived from the atomic energy. As shown in Figure 3, the adsorption energy exhibits nonlinear behavior on the high-energy side, suggesting that the adsorption energy of the CO molecule does not solely depend on the atomic energy. This behavior can be attributed to the coordination number per adsorption site, where corners and edges exhibit a coordination number of 6 and 7, respectively, and facets exhibit a value of 8 or 9. Higher coordination numbers are more susceptible to the influence of the surrounding environment. One possible solution to address this non-trivial nonlinearity is to incorporate the results of direct adsorption energy calculations for binary and multiple systems into the regression analysis. More reliable predictions can be achieved using nonlinear regressions based on kernel learning and neural network methods, incorporating certain direct evaluations of adsorption energies of CO on the HEA environment.

To learn the nonlinearity, we applied KRR and QNNR [60] to construct an adsorption energy correction model for each elemental species at the adsorption site of HEA NP. This model takes the *LSE*-predicted adsorption energy as the input and outputs an adsorption energy close to the correct value. Figure 6 shows the correlation plot between the corrected values and correct values for the adsorption energies of CO on 14 patterns of HEA NPs by the regression model using KRR and QNNR. The RMSEs of the adsorption energy predictions for all adsorption sites by the KRR and QNNR models are 0.0580 eV and

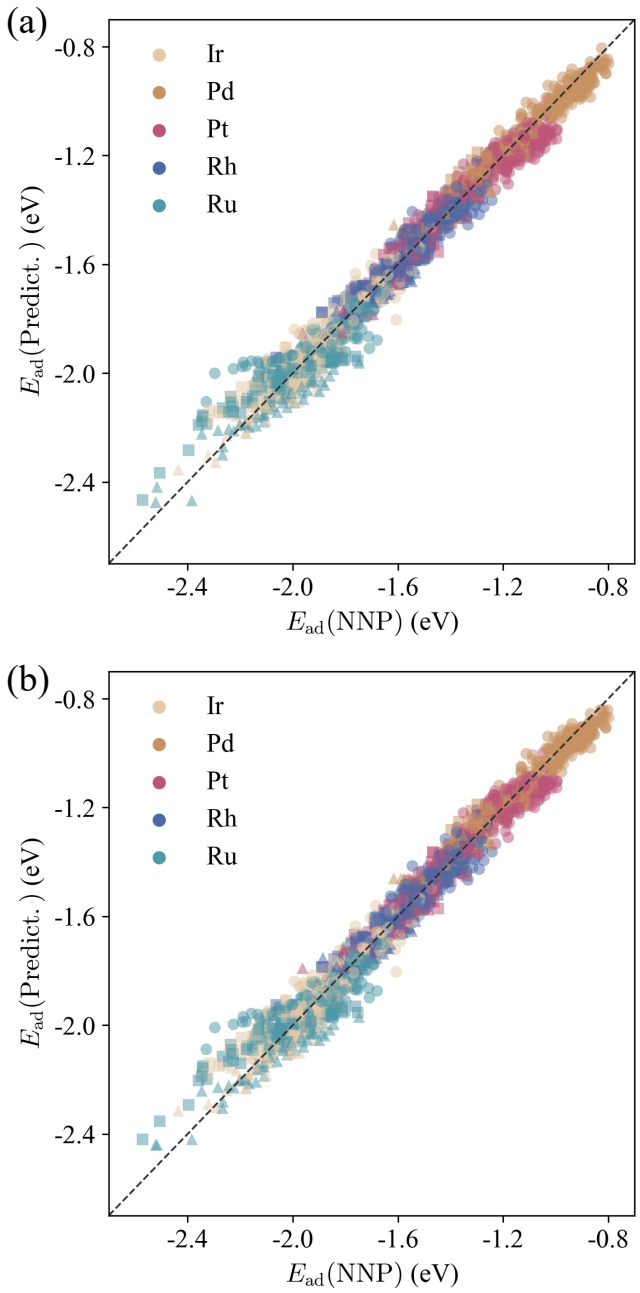

Figure 6. Correlation plots of CO adsorption energies for each element (Ir, Pd, Pt, Rh, Ru) for 14 patterns of IrPdPtRhRu HEA_{201} NPs. The energies are corrected using nonlinear regression models based on (a) KRR and (b) QNNR. These values are plotted against directly obtained values by NNP, which serve as the standard for accuracy.

0.0579 eV, respectively, indicating comparable nonlinear regression performance. Compared with the uncorrected LSE predictions, the RMSE values improve by approximately three times.

V. DISCUSSION

We utilize the atomic energy obtained from the NNPs and introduce a metric named LSE, representing the surface energy per atom. Using the LSE, we determine the adsorption energy of CO molecules on the on-top site of IrPdPtRhRu HEA_{201} NPs with a large number of atomic combinations as a distribution, as shown in Figure 3(b). This approach offers a novel means of analyzing atomic energies to evaluate various adsorption energies in multicomponent systems such as the vast number of of atomic configurations found in HEA environments. In other words, the adsorption energy distribution obtained by LSE prediction can help effectively visualize the unexpected cocktail effects induced by the complex environment of HEA NPs.

Notably, our calculations solely consider the adsorption energies on monometallic NPs and isolated multicomponent NPs, without the need for direct evaluation of the CO molecular adsorption energy on the HEA itself. This approach enables the evaluation of adsorption energies approximately 10^5 times faster than DFT direct evaluations, facilitating the visualization of the cocktail effect. In terms of accuracy (Figure 5), a comparison with DFT calculations reveals that the predictions by LSE are nearly an order of magnitude larger than the chemical accuracy, although they are not quantitatively accurate. Nonetheless, the relative energies exhibit a similar trend, indicating that qualitative comparisons that consider the influence of the surrounding environment for each element are feasible. Consequently, this method can be employed as a screening tool prior to applying DFT calculations or high-level quantum chemical methods such as CC or MBPT.

Figure 4(b) shows a parity plot between the LSE predicted- and directly evaluated adsorption energies. The prediction is highly accurate, with an RMSE of 0.150 eV relative to the correct values, despite its low cost compared with those of direct evaluations. However, nonlinearity relative to the correct values is observed, indicating nonlinear behavior with respect to LSE. We introduce a naive method to capture this nonlinearity: nonlinear regression between the directly evaluated CO adsorption energy and the predictions. We model nonlinear regression with KRR and the classical quantum hybrid algorithm QNNR. Learning the adsorption energies for only 732 sites for NPs in six patterns of structures improves the resulting LSE predictions by three times for the remaining 14 patterns tested for 1708 sites. The constraint that the norm of the parameters in QNNR must be 1 is expected to act as a regularization. Results of the KRR and QNNR models demonstrate their similar regularization capabilities. Although our adsorption energy correction model does not inherently requires quantum computing, its utility may extend to a wider chemical space and the construction of models encompassing the entire periodic table.

Finally, we discuss the potential applications of the proposed method for chemical reaction design for catalyst and device development. Previous studies have examined the role of atomic energy in improving the accuracy and efficiency of NNPs and validated atomic energy mapping results [57, 73–76]. More recently, researchers have attempts to gain chemical insights from atomic energies [77]. However, to the best of our knowledge, the LSE prediction method proposed in this study is the first to provide evidence that atomic energy can serve as a descriptor for efficiently evaluating chemical quantities. Moreover, unlike atomic energies, which are absolute quantities, LSEs are relative quantities and are thus expected to be less sensitive to differences in computational methods, such as the treatment of basis functions and inner-shell electrons. Therefore, this approach can facilitate chemical reaction design for machine-learning-based material design, which has garnered significant interest in recent years [78–80].

VI. CONCLUSION

In this work, we have introduced a computational methodology to predict molecular adsorption energies on HEAs using the LSE descriptor, derived from atomic energies calculated by NNPs. This method addresses the challenge of evaluating the vast chemical space of HEAs due to their compositional diversity and the computational expense associated with direct DFT and NNP calculations. The LSE descriptor efficiently captures the local reactivity of surface atoms, allowing for the rapid and accurate prediction of adsorption energies across a wide range of HEA configurations.

Our approach significantly accelerates the computational process, reducing the time from hundreds of years with DFT and hundreds of days with NNP to just a few hours, making it a practical tool for material discovery and catalyst design. The adoption of nonlinear regression techniques, combined with advanced machine learning models such as KRR and QNNR, has improved the accuracy of adsorption energy predictions, even in the face of nonlinearity inherent in multicomponent systems.

The successful application of the newly introduced LSE descriptor in this study showcases its potential for material simulation, offering a scalable and efficient way to explore the catalytic properties of HEAs. This research not only paves the way for rapid and accurate computational screening of catalytic materials but also sets the stage for the development of new computational tools that can handle the complexities of modern material science, particularly in the realm of high-entropy materials.

ACKNOWLEDGMENTS

We thank Nobuki Inoue and Tuan Minh Do for fruitful discussions. This project was supported by funding from the MEXT Quantum Leap Flagship Program (MEXT-QLEAP) through Grant No. JPMXS0120319794, and the JST COI-NEXT Program through Grant No. JPMJPF2014. The completion of this research was partially facilitated by the JSPS Grants-in-Aid for Scientific Research (KAKENHI), specifically Grant Nos. JP23H03819 and JP21K18933. We thank the Supercomputer Center, the Institute for Solid State Physics, the University of Tokyo for the use of the facilities. This work was also achieved through the use of SQUID at the Cybermedia Center, Osaka University.

[1] B. Cantor, I. Chang, P. Knight, and A. Vincent, Microstructural development in equiatomic multicomponent alloys, Materials Science and Engineering: A **375**, 213 (2004).

[2] J.-W. Yeh, S.-K. Chen, S.-J. Lin, J.-Y. Gan, T.-S. Chin, T.-T. Shun, C.-H. Tsau, and S.-Y. Chang, Nanostructured high-entropy alloys with multiple principal elements: novel alloy design concepts and outcomes, Advanced engineering materials **6**, 299 (2004).

[3] E. J. Pickering and N. G. Jones, High-entropy alloys: a critical assessment of their founding principles and future prospects, International Materials Reviews **61**, 183 (2016).

[4] E. P. George, D. Raabe, and R. O. Ritchie, High-entropy alloys, Nature Reviews Materials **4**, 515 (2019).

[5] B. Cao, C. Wang, T. Yang, and C. Liu, Cocktail effects in understanding the stability and properties of face-centered-cubic high-entropy alloys at ambient and cryogenic temperatures, Scripta Materialia **187**, 250 (2020).

[6] D. Wu, K. Kusada, T. Yamamoto, T. Toriyama, S. Matsumura, I. Gueye, O. Seo, J. Kim, S. Hiroi, O. Sakata, S. Kawaguchi, Y. Kubota, and H. Kitagawa, On the electronic structure and hydrogen evolution reaction activity of platinum group metal-based high-entropy-alloy nanoparticles, Chemical Science **11**, 12731 (2020).

[7] D. Wu, K. Kusada, T. Yamamoto, T. Toriyama, S. Matsumura, S. Kawaguchi, Y. Kubota, and H. Kitagawa, Platinum-group-metal high-entropy-alloy nanoparticles, Journal of the American Chemical Society **142**, 13833 (2020).

[8] K. Kusada, D. Wu, and H. Kitagawa, New aspects of platinum group metal-based solid-solution alloy nanoparticles: Binary to high-entropy alloys, Chemistry – A European Journal **26**, 5105 (2020).

[9] D. Wu, K. Kusada, Y. Nanba, M. Koyama, T. Yamamoto, T. Toriyama, S. Matsumura, O. Seo, I. Gueye, J. Kim, *et al.*, Noble-metal high-entropy-alloy nanoparticles: atomic-level insight into the electronic structure, Journal of the American Chemical Society **144**, 3365 (2022).

[10] T. A. Batchelor, J. K. Pedersen, S. H. Winther, I. E. Castelli, K. W. Jacobsen, and J. Rossmeisl, High-entropy alloys as a discovery platform for electrocatalysis, Joule **3**, 834 (2019).

[11] H. S. Oh, S. J. Kim, K. Odbadrakh, W. H. Ryu, K. N. Yoon, S. Mu, F. Körmann, Y. Ikeda, C. C. Tasan, D. Raabe, T. Egami, and E. S. Park, Engineering atomic-level complexity in high-entropy and complex concentrated alloys, Nature Communications **10**, 10.1038/s41467-019-10012-7 (2019).

[12] W. Huo, S. Wang, F. J. Dominguez-Gutierrez, K. Ren, Ł. Kurpaska, F. Fang, S. Papanikolaou, H. S. Kim, and J. Jiang, High-entropy materials for electrocatalytic applications: a review of first principles modeling and simulations, Materials Research Letters **11**, 713 (2023).

[13] J. K. Nørskov, F. Abild-Pedersen, F. Studt, and T. Bligaard, Density functional theory in surface chemistry and catalysis, Proceedings of the National Academy of Sciences **108**, 937 (2011).

[14] N. Mardirossian and M. Head-Gordon, Thirty years of density functional theory in computational chemistry: an overview and extensive assessment of 200 density functionals, Molecular physics **115**, 2315 (2017).

[15] T. Shiota, W. Mizukami, H. Tochihara, K. Yagyu, T. Suzuki, and Y. Aoki, Microscopic hopping mechanism of an isolated PTCDA molecule on a reactive ge(001) surface, The Journal of Physical Chemistry C **124**, 24704 (2020).

[16] J. McClain, Q. Sun, G. K.-L. Chan, and T. C. Berkelbach, Gaussian-based coupled-cluster theory for the ground-state and band structure of solids, Journal of chemical theory and computation **13**, 1209 (2017).

[17] T. Gruber, K. Liao, T. Tsatsoulis, F. Hummel, and A. Grüneis, Applying the coupled-cluster ansatz to solids and surfaces in the thermodynamic limit, Physical Review X **8**, 021043 (2018).

[18] I. Y. Zhang and A. Grüneis, Coupled cluster theory in materials science, Frontiers in Materials **6**, 123 (2019).

[19] I. Shavitt and R. J. Bartlett, *Many-body methods in chemistry and physics: MBPT and coupled-cluster theory* (Cambridge university press, 2009).

[20] L. Schimka, J. Harl, A. Stroppa, A. Grüneis, M. Marsman, F. Mittendorfer, and G. Kresse, Accurate surface and adsorption energies from many-body perturbation theory, Nature materials **9**, 741 (2010).

[21] T. Bligaard, J. Nørskov, S. Dahl, J. Matthiesen, C. Christensen, and J. Sehested, The brønsted–evans–polanyi relation and the volcano curve in heterogeneous catalysis, Journal of Catalysis **224**, 206 (2004).

[22] A. J. Medford, A. Vojvodic, J. S. Hummelshøj, J. Voss, F. Abild-Pedersen, F. Studt, T. Bligaard, A. Nilsson, and J. K. Nørskov, From the sabatier principle to a predictive theory of transition-metal heterogeneous catalysis, Journal of Catalysis **328**, 36 (2015).

[23] J. Behler and M. Parrinello, Generalized neural-network representation of high-dimensional potential-energy surfaces, Physical Review Letters **98**, 10.1103/physrevlett.98.146401 (2007).

[24] J. Behler, Atom-centered symmetry functions for constructing high-dimensional neural network potentials, The Journal of Chemical Physics **134**, 074106 (2011).

[25] J. Behler, Constructing high-dimensional neural network potentials: a tutorial review, International Journal of Quantum Chemistry **115**, 1032 (2015).

[26] J. S. Smith, O. Isayev, and A. E. Roitberg, ANI-1: an extensible neural network potential with DFT accuracy at force field computational cost, Chemical Science **8**, 3192 (2017).

[27] K. Lee, D. Yoo, W. Jeong, and S. Han, SIMPLE-NN: An efficient package for training and executing neural-network interatomic potentials, Computer Physics Communications **242**, 95 (2019).

[28] J. Gilmer, S. S. Schoenholz, P. F. Riley, O. Vinyals, and G. E. Dahl, Neural message passing for quantum chemistry (2017), arXiv:1704.01212 [cs.LG].

[29] K. T. Schütt, H. E. Sauceda, P.-J. Kindermans, A. Tkatchenko, and K.-R. Müller, SchNet – a deep learning architecture for molecules and materials, The Journal of Chemical Physics **148**, 241722 (2018).

[30] K. T. Schütt, H. E. Sauceda, P.-J. Kindermans, A. Tkatchenko, and K.-R. Müller, Schnet–a deep learning architecture for molecules and materials, The Journal of Chemical Physics **148** (2018).

[31] T. Xie and J. C. Grossman, Crystal graph convolutional neural networks for an accurate and interpretable prediction of material properties, Physical Review Letters **120**, 10.1103/physrevlett.120.145301 (2018).

[32] C. Chen, W. Ye, Y. Zuo, C. Zheng, and S. P. Ong, Graph networks as a universal machine learning framework for molecules and crystals, Chemistry of Materials **31**, 3564 (2019).

[33] C. L. Zitnick, A. Das, A. Kolluru, J. Lan, M. Shuaibi, A. Sriram, Z. Ulissi, and B. Wood, Spherical channels for modeling atomic interactions (2022), arXiv:2206.14331 [physics.chem-ph].

[34] C. Chen and S. P. Ong, A universal graph deep learning interatomic potential for the periodic table, Nature Computational Science **2**, 718 (2022).

[35] S. Takamoto, C. Shinagawa, D. Motoki, K. Nakago, W. Li, I. Kurata, T. Watanabe, Y. Yayama, H. Iriguchi, Y. Asano, *et al.*, Towards universal neural network potential for material discovery applicable to arbitrary combination of 45 elements, Nature Communications **13**, 2991 (2022).

[36] I. Batatia, D. P. Kovacs, G. Simm, C. Ortner, and G. Csányi, Mace: Higher order equivariant message passing neural networks for fast and accurate force fields, Advances in Neural Information Processing Systems **35**, 11423 (2022).

[37] B. Deng, P. Zhong, K. Jun, J. Riebesell, K. Han, C. J. Bartel, and G. Ceder, Chgnet as a pretrained universal neural network potential for charge-informed atomistic modelling, Nature Machine Intelligence , 1–11 (2023).

[38] J. Gasteiger, M. Shuaibi, A. Sriram, S. Günnemann, Z. Ulissi, C. L. Zitnick, and A. Das, Gemnet-oc: developing graph neural networks for large and diverse molecular simulation datasets, arXiv preprint arXiv:2204.02782 (2022).

[39] R. Tran, J. Lan, M. Shuaibi, B. M. Wood, S. Goyal, A. Das, J. Heras-Domingo, A. Kolluru, A. Rizvi, N. Shoghi, *et al.*, The open catalyst 2022 (oc22) dataset and challenges for oxide electrocatalysts, ACS Catalysis **13**, 3066 (2023).

[40] D. P. Kovács, J. H. Moore, N. J. Browning, I. Batatia, J. T. Horton, V. Kapil, I.-B. Magdău, D. J. Cole, and G. Csányi, Mace-off23: Transferable machine learning force fields for organic molecules, arXiv preprint arXiv:2312.15211 (2023).

[41] I. Batatia, P. Benner, Y. Chiang, A. M. Elena, D. P. Kovács, J. Riebesell, X. R. Advincula, M. Asta, W. J. Baldwin, N. Bernstein, A. Bhowmik, S. M. Blau, V. Cărare, J. P. Darby, S. De, F. D. Pia, V. L. Deringer, R. Elijošius, Z. El-Machachi, E. Fako, A. C. Ferrari, A. Genreith-Schriever, J. George, R. E. A. Goodall, C. P. Grey, S. Han, W. Handley, H. H. Heenen, K. Hermansson, C. Holm, J. Jaafar, S. Hofmann, K. S. Jakob, H. Jung, V. Kapil, A. D. Kaplan, N. Karimitari, N. Kroupa, J. Kullgren, M. C. Kuner, D. Kuryla, G. Liepuoniute, J. T. Margraf, I.-B. Magdău, A. Michaelides, J. H. Moore, A. A. Naik, S. P. Niblett, S. W. Norwood, N. O'Neill, C. Ortner, K. A. Persson, K. Reuter, A. S. Rosen, L. L. Schaaf, C. Schran, E. Sivonxay, T. K. Stenczel, V. Svahn, C. Sutton, C. van der Oord, E. Varga-Umbrich, T. Vegge, M. Vondrák, Y. Wang, W. C. Witt, F. Zills, and G. Csányi, A foundation model for atomistic materials chemistry (2023), arXiv:2401.00096 [physics.chem-ph].

[42] A. Musaelian, S. Batzner, A. Johansson, L. Sun, C. J. Owen, M. Kornbluth, and B. Kozinsky, Learning local equivariant representations for large-scale atomistic dynamics, Nature Communications **14**, 579 (2023).

[43] Y.-L. Liao, B. Wood, A. Das, and T. Smidt, Equiformerv2: Improved equivariant transformer for scaling to higher-degree representations, arXiv preprint arXiv:2306.12059 (2023).

[44] A. Merchant, S. Batzner, S. S. Schoenholz, M. Aykol, G. Cheon, and E. D. Cubuk, Scaling deep learning for materials discovery, Nature **624**, 80 (2023).

[45] C. M. Clausen, J. Rossmeisl, and Z. W. Ulissi, Adapting oc20-trained equiformerv2 models for high-entropy materials, arXiv preprint arXiv:2403.09811 (2024).

[46] J. Dean, M. G. Taylor, and G. Mpourmpakis, Unfolding adsorption on metal nanoparticles: Connecting stability with catalysis, Science advances **5**, eaax5101 (2019).

[47] Y. Nanba and M. Koyama, An element-based generalized coordination number for predicting the oxygen binding energy on pt3m (m= co, ni, or cu) alloy nanoparticles, ACS omega **6**, 3218 (2021).

[48] Z. Lu, Z. W. Chen, and C. V. Singh, Neural network-assisted development of high-entropy alloy catalysts: decoupling ligand and coordination effects, Matter **3**, 1318 (2020).

[49] Z. Yang and W. Gao, Applications of machine learning in alloy catalysts: rational selection and future development of descriptors, Advanced Science **9**, 2106043 (2022).

[50] M. Tamtaji, S. Chen, Z. Hu, W. A. G. III, and G. Chen, A surrogate machine learning model for the design of single-atom catalyst on carbon and porphyrin supports towards electrochemistry, The Journal of Physical Chemistry C 10.1021/acs.jpcc.3c00765 (2023).

[51] K. Momma and F. Izumi, *VESTA3* for three-dimensional visualization of crystal, volumetric and morphology data, Journal of Applied Crystallography **44**, 1272 (2011).

[52] H. Nakai, Energy density analysis with kohn–sham orbitals, Chemical Physics Letters **363**, 73 (2002).

[53] Y. Kikuchi, Y. Imamura, and H. Nakai, One-body en-

ergy decomposition schemes revisited: Assessment of mulliken-, grid-, and conventional energy density analyses, International Journal of Quantum Chemistry **109**, 2464 (2009).

[54] M. Yu, D. R. Trinkle, and R. M. Martin, Energy density in density functional theory: Application to crystalline defects and surfaces, Physical Review B **83**, 10.1103/physrevb.83.115113 (2011).

[55] Y. Huang, J. Kang, W. A. Goddard, and L.-W. Wang, Density functional theory based neural network force fields from energy decompositions, Physical Review B **99**, 10.1103/physrevb.99.064103 (2019).

[56] J. J. Eriksen, Mean-field density matrix decompositions, The Journal of Chemical Physics **153**, 214109 (2020).

[57] D. Yoo, K. Lee, W. Jeong, D. Lee, S. Watanabe, and S. Han, Atomic energy mapping of neural network potential, Physical Review Materials **3**, 10.1103/physrevmaterials.3.093802 (2019).

[58] H. An, H. Ha, M. Yoo, and H. Y. Kim, Understanding the atomic-level process of co-adsorption-driven surface segregation of pd in (aupd) 147 bimetallic nanoparticles, Nanoscale **9**, 12077 (2017).

[59] L. Vega, J. Garcia-Cardona, F. Viñes, P. L. Cabot, and K. M. Neyman, Nanostructuring determines poisoning: tailoring CO adsorption on PtCu bimetallic nanoparticles, Materials Advances **3**, 4159 (2022).

[60] K. Mitarai, M. Negoro, M. Kitagawa, and K. Fujii, Quantum circuit learning, Physical Review A **98**, 10.1103/physreva.98.032309 (2018).

[61] S. R. Bahn and K. W. Jacobsen, An object-oriented scripting interface to a legacy electronic structure code, Comput. Sci. Eng. **4**, 56 (2002).

[62] A. H. Larsen, J. J. Mortensen, J. Blomqvist, I. E. Castelli, R. Christensen, M. Dułak, J. Friis, M. N. Groves, B. Hammer, C. Hargus, E. D. Hermes, P. C. Jennings, P. B. Jensen, J. Kermode, J. R. Kitchin, E. L. Kolsbjerg, J. Kubal, K. Kaasbjerg, S. Lysgaard, J. B. Maronsson, T. Maxson, T. Olsen, L. Pastewka, A. Peterson, C. Rostgaard, J. Schiøtz, O. Schütt, M. Strange, K. S. Thygesen, T. Vegge, L. Vilhelmsen, M. Walter, Z. Zeng, and K. W. Jacobsen, The atomic simulation environment—a python library for working with atoms, Journal of Physics: Condensed Matter **29**, 273002 (2017).

[63] K. Kusada, H. Kobayashi, T. Yamamoto, S. Matsumura, S. Naoya, K. Sato, K. Nagaoka, Y. Kubota, and H. Kitagawa, Discovery of face-centered-cubic ruthenium nanoparticles: Facile size-controlled synthesis using the chemical reduction method, Journal of the American Chemical Society **135**, 5493 (2013).

[64] G. Kresse and J. Hafner, Ab initio molecular dynamics for open-shell transition metals, Physical Review B **48**, 13115 (1993).

[65] G. Kresse and J. Furthmüller, Efficient iterative schemes for ab initio total-energy calculations using a plane-wave basis set, Phys. Rev. B **54**, 11169 (1996).

[66] G. Kresse and J. Furthmüller, Efficiency of ab-initio total energy calculations for metals and semiconductors using a plane-wave basis set, Computational Materials Science **6**, 15 (1996).

[67] J. P. Perdew, K. Burke, and M. Ernzerhof, Generalized gradient approximation made simple, Physical Review Letters **77**, 3865 (1996).

[68] P. E. Blöchl, Projector augmented-wave method, Physical Review B **50**, 17953 (1994).

[69] G. Kresse and D. Joubert, From ultrasoft pseudopotentials to the projector augmented-wave method, Physical Review B **59**, 1758 (1999).

[70] F. Pedregosa, G. Varoquaux, A. Gramfort, V. Michel, B. Thirion, O. Grisel, M. Blondel, P. Prettenhofer, R. Weiss, V. Dubourg, J. Vanderplas, A. Passos, D. Cournapeau, M. Brucher, M. Perrot, and E. Duchesnay, Scikit-learn: Machine learning in Python, Journal of Machine Learning Research **12**, 2825 (2011).

[71] `https://github.com/Qulacs-Osaka/scikit-qulacs`.

[72] Y. Suzuki, Y. Kawase, Y. Masumura, Y. Hiraga, M. Nakadai, J. Chen, K. M. Nakanishi, K. Mitarai, R. Imai, S. Tamiya, T. Yamamoto, T. Yan, T. Kawakubo, Y. O. Nakagawa, Y. Ibe, Y. Zhang, H. Yamashita, H. Yoshimura, A. Hayashi, and K. Fujii, Qulacs: a fast and versatile quantum circuit simulator for research purpose, Quantum **5**, 559 (2021).

[73] W. Jeong, D. Yoo, K. Lee, J. Jung, and S. Han, Efficient atomic-resolution uncertainty estimation for neural network potentials using a replica ensemble, The Journal of Physical Chemistry Letters **11**, 6090 (2020).

[74] S. Watanabe, W. Li, W. Jeong, D. Lee, K. Shimizu, E. Mimanitani, Y. Ando, and S. Han, High-dimensional neural network atomic potentials for examining energy materials: some recent simulations, Journal of Physics: Energy **3**, 012003 (2020).

[75] H. A. Doan, C. Li, L. Ward, M. Zhou, L. A. Curtiss, and R. S. Assary, Accelerating the evaluation of crucial descriptors for catalyst screening via message passing neural network, Digital Discovery **2**, 59 (2023).

[76] S. Chong, F. Grasselli, C. B. Mahmoud, J. D. Morrow, V. L. Deringer, and M. Ceriotti, Robustness of local predictions in atomistic machine learning models (2023), arXiv:2306.15638 [physics.chem-ph].

[77] F. Ø. Kjeldal and J. J. Eriksen, Decomposing chemical space: Applications to the machine learning of atomic energies, Journal of Chemical Theory and Computation **19**, 2029 (2023).

[78] M. Meuwly, Machine learning for chemical reactions, Chemical Reviews **121**, 10218 (2021).

[79] M. Wen, E. W. C. Spotte-Smith, S. M. Blau, M. J. McDermott, A. S. Krishnapriyan, and K. A. Persson, Chemical reaction networks and opportunities for machine learning, Nature Computational Science **3**, 12 (2023).

[80] T. Shiota, K. Ishihara, and W. Mizukami, Universal neural network potentials as descriptors: Towards scalable chemical property prediction using quantum and classical computers, arXiv preprint arXiv:2402.18433 (2024).